ELSEVIER

International Journal of Solids and Structures 41 (2004) 2501–2519

INTERNATIONAL JOURNAL OF SOLIDS and STRUCTURES

www.elsevier.com/locate/ijsolstr

Electro-elastic stress analysis for a Zener–Stroh crack at the metal/piezoelectric bi-material interface

Z.M. Xiao *, J.F. Zhao

Center for Mechanics of Micro-Systems, School of Mechanical and Production Engineering, Nanyang Technological University, Singapore 639798, Singapore

Received 6 June 2003; received in revised form 13 November 2003

Abstract

A Zener–Stroh crack may nucleate at the interface of metal/piezoelectric bi-materials, when piled-up dislocations along a slip plane in metal material are stopped by the interface which works as an obstacle. As a kind of microcrack, Zener–Stroh crack controls the initial phase of crack nucleation. In the first step of our current research, the stress and electric displacement fields for a single interfacial dislocation in general piezoelectric/metal bimaterials are obtained in an explicit close form. With this solution as the Green function, the interfacial Zener–Stroh crack problem is formulated into a set of singular integral equations with distributed dislocation technique. These singular integral equations are then solved by numerical method based on the singularity nature at the crack tips. To deal with the oscillation behaviors near the interfacial crack tips, both open crack tip model and contact zone model are considered and compared each other in the paper. Solutions on the stress field, stress and electric displacement intensity factors and contact zone length are obtained. A numerical example of a Zener–Stroh crack at the Pt/PZT-5H bimaterial interface is given. Some useful electro-elastic characteristics related to the crack are found and discussed.

Keywords: Zener–Stroh crack; Interface; Piezoelectric material; Stress and electric displacement (SED)

1. Introduction

1.1. Metal/piezoelectric structure

As a typical smart material, piezoelectric ceramics (generally, lead zirconate titanate or PZT in short) are widely used in sensors, transducers and actuators, some of which are implemented through micro-electro-mechanical-systems (MEMS). Often bonded to a piezoelectric layer, metal electrodes (generally Cu or Pt) supply the voltage across the piezoelectric material and also act as a template to ensure the correct crystallographic alignment of the piezoelectric film as the same time. Due to the material mismatch, thermal stress as well as residual stress and even electric field may induce microcrack nucleation along the interface.

* Corresponding author. Tel.: +65-6790-4726; fax: +65-6791-1859/+65-6792-1859.
E-mail address: mzxiao@ntu.edu.sg (Z.M. Xiao).

0020-7683/$ - see front matter © 2003 Elsevier Ltd. All rights reserved.
doi:10.1016/j.ijsolstr.2003.12.008

For polycrystalline metal material, dislocations may pile up along a slip plane until they are stopped by an obstacle such as an interface and thus coalesce into a microcrack due to Zener–Stroh crack initiation mechanism (Zener, 1948; Stroh, 1954), as shown in Fig. 1. Such type of microcracks is very often observed in metal matrix composite materials.

1.2. Nucleation of a Zener–Stroh crack

Zener–Stroh mechanism of microcrack nucleation was first proposed by Zener (1948) and later further developed by Stroh (1954), therefore the crack is named after those two researchers as Zener–Stroh crack. According to Stroh's (1954) research result, a number of 10^3 dislocations are needed to form a crack in hardened copper and a number of the order of 10^2 is required if a stack of piled-up dislocations on parallel slip planes exist. Through energy consideration, Stroh (1955) argued that the energy needed to initiate a Zener–Stroh crack is possibly lower than that due to other mechanism. From then on, a lot of crack models proposed by subsequent researchers can be regarded as the variants of Zener–Stroh crack. Cottrell (1958) suggested that dislocations piling up along two intersecting slip planes could coalesce into a microcrack. Another model of crack nucleation can be called anti-Zener–Stroh mechanism proposed by Kikuchi et al. (1981). In this model, concentrated stress field makes a slip nucleated near the end of a particle at a grain boundary, dislocations of one sign move away from this region, a crack is then initiated as a pileup of the left opposite sign dislocations.

Zener–Stroh crack and Griffith crack are a complementary pair which have opposite characteristics. Physical parameters symmetric for the Griffith crack are anti-symmetric for Zener–Stroh crack, and vice versa. For example, anti-symmetric dislocation distribution along the Griffith crack causes symmetric traction stress, while dislocation distribution along a Zener–Stroh crack is symmetric and the stress field is anti-symmetric as a result. Weertman (1986) compared Griffith crack and Zener–Stroh crack on the stress, displacement, dislocation density and stress intensity factors. It is worth to mention that the total sum of Burgers vectors of the dislocations b^{T} in a Zener–Stroh crack is not equal to zero due to displacement loading mechanism. This is different to a Griffith crack where the total sum of Burgers vectors of the dislocations along the crack line is zero.

In recent years, Zener–Stroh crack problems were widely investigated in linear elastic fracture mechanics (LEFM) context. An interfacial Zener–Stroh crack problem was solved by Cherepanov (1994) for isotropic elastic material and by Fan (1994) for anisotropic elastic material. Based on their results, there is oscillation behavior near the crack tip. Later on the contact zone model was employed to reformulate the problem (Fan et al., 1998), and oscillation behavior was ceased successfully. It was found that the contact zone length could be fairly large for shear-load dominant case. The stress investigation on interfacial Zener–Stroh crack in multi-layered thin-film structures was carried out by Xiao and Zhao (submitted for publication). The interaction between a Zener–Stroh crack and a coated inclusion (Xiao and Chen, 2001) were investigated around the same period. Zener–Stroh crack mechanism was also used to explain fatigue fracture procedure in various materials, such as silicon carbide (Shih et al., 2000) and metal fatigue (Lawson et al., 1997).

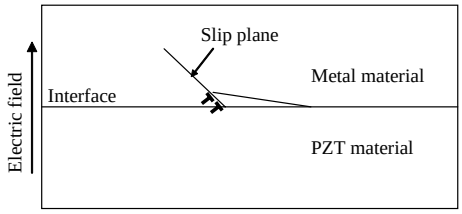

Fig. 1. Zener–Stroh crack nucleation mechanism along metal/piezoelectric bi-material interface.

1.3. Crack problems in piezoelectric materials

With the increasing application of piezoelectric materials, a lot of efforts have been made in solving various mechanics problems in piezoelectric materials (Huang and Kuang, 2001; Pak, 1992; Park and Sun, 1995; Sosa, 1992; Qin and Mai, 1998; Suo et al., 1992). In general fractures always happen along the interface since it is weaker than the interior of the material, interfacial crack problems in piezoelectric material were solved repeatedly in recent years (Shen et al., 2000; Gao and Yu, 1998; Zhang and Tong, 1996; Qin and Yu, 1997). However, to the best knowledge of the authors so far, few publications can be found on the electro-elastic characteristics of interfacial Zener–Stroh crack in piezoelectric layered structures or composite materials. In the current paper, stress investigation on an interfacial Zener–Stroh crack along a metal/piezoelectric interface has been carried out. To deal with the oscillation behaviors in front of the interfacial crack tips, both open crack tip model and contact zone model are considered. Solutions on the stress field, stress and electric displacement intensity factors (SEDIFs) and contact zone length are obtained. Some useful electro-elastic characteristics of the crack are found and discussed.

2. Formulation

The physical problem to be solved is illustrated in Fig. 2. Along the interface is a Zener–Stroh crack, whose crack tip where the dislocation enters the crack is called the blunt tip, while the other one is called the sharp tip. A Zener–Stroh crack always propagates from the sharp tip. The crack length is $2a$. In the Cartesian coordinate system, the y-axis perpendicularly crosses the centre of the crack with x-axis along the interface. The electric field is added along the y-direction. To formulate the problem with distributed dislocation technique, we first derive the stress and electric displacement (SED) field due to a single dislocation at the interface of the two bonded general piezoelectric materials. With the single dislocation solution as a Green function, the crack problem is then formulated with the aid of distributed dislocation based fracture mechanics theory. Both open crack tip model and contact zone model for the crack formulation are considered in our study.

2.1. Stroh's formulism

Formulation models for anisotropic bimaterials were developed by Lekhnitskii (1963) and Stroh (1958) independently, both create equal results. In the current problem, Stroh's formulism is adopted. It begins with the constitutive equations for general piezoelectric materials:

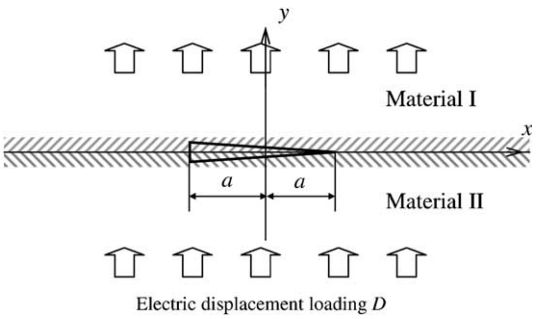

Fig. 2. A Zener–Stroh crack at the interface.

$$\sigma_{ij} = c_{ijkl}u_{k,l} - e_{lij}\varphi_{,l}, \tag{1}$$

$$D_i = e_{ikl}u_{k,l} + \kappa_{il}\varphi_{,l}, \tag{2}$$

where e_{lij} are the piezoelectric coefficients measured at a constant electric field; u and σ are the mechanical displacements and stresses, respectively; φ and D_i are the electric potential and displacements, respectively; κ_{il} are the dielectric constants measured at a constant strain and temperature. For manipulation convenience, the compact form of Eqs. (1) and (2) can be written as

$$\Pi_{iJ} = E_{iJKl}U_{K,l} \tag{3}$$

with

$$\Pi_{iJ} = \begin{cases} \sigma_{ij}, & i,J = 1,2,3, \\ D_i, & J = 4;\ i = 1,2,3, \end{cases} \tag{4}$$

$$\mathbf{U}_K = \begin{cases} u_k, & K = 1,2,3, \\ \varphi, & K = 4, \end{cases} \tag{5}$$

$$E_{iJKl} = \begin{cases} c_{ijkl}, & i,J,K,l = 1,2,3, \\ e_{lij}, & K = 4;\ i,J,l = 1,2,3, \\ e_{ikl}, & J = 4;\ i,K,l = 1,2,3, \\ -\kappa_{il}, & J = K = 4;\ i,l = 1,2,3, \end{cases} \tag{6}$$

Eq. (5) is the generalized displacement function vector and can be written as

$$\mathbf{U} = [u_1, u_2, u_3, \varphi]^{\mathrm{T}}, \tag{7}$$

and the stress and electric displacement (SED) components of $\mathbf{\Pi}_2$ is in forms of

$$\mathbf{\Pi}_2 = [\Pi_{21}, \Pi_{22}, \Pi_{23}, \Pi_{24}]^{\mathrm{T}}. \tag{8}$$

Without body forces and free charges, equilibrium can then be written as

$$\Pi_{iJ,i} = 0. \tag{9}$$

The general solution of (9) for generalized two-dimensional problem can be expressed as (Suo et al., 1992)

$$\mathbf{U} = \mathbf{A}\mathbf{f}(z) + \overline{\mathbf{A}}\overline{\mathbf{f}}(z), \tag{10}$$

$$\mathbf{\Pi}_2 = \mathbf{B}\mathbf{f}'(z) + \overline{\mathbf{B}}\overline{\mathbf{f}}'(z) \tag{11}$$

with

$$z = x + py, \tag{12}$$

where $\mathbf{A}$ and $\mathbf{B}$ are 4×4 complex matrices,

$$\mathbf{A} = [\mathbf{a}_1, \mathbf{a}_2, \mathbf{a}_3, \mathbf{a}_4], \quad \mathbf{B} = [\mathbf{b}_1, \mathbf{b}_2, \mathbf{b}_3, \mathbf{b}_4], \tag{13}$$

and

$$\mathbf{f}(\mathbf{z}) = [f_1(z_1), f_2(z_2), f_3(z_3), f_4(z_4)]^{\mathrm{T}}. \tag{14}$$

To determine p and $\mathbf{a}$, substituting Eq. (10) into Eqs. (3) and (9), we can obtain the eigenvalues p_j and eigenvectors $\mathbf{a}_j$ from the following equation:

$$[\mathbf{Q} + p_j(\mathbf{R} + \mathbf{R}^{\mathrm{T}}) + p_j^2\mathbf{T}]\mathbf{a}_j = 0, \tag{15}$$

which leads to

$$\left\|\mathbf{Q}+p_j(\mathbf{R}+\mathbf{R}^{\mathrm{T}})+p_j^2\mathbf{T}\right\|=0, \tag{16}$$

where $\mathbf{Q}$, $\mathbf{R}$ and $\mathbf{T}$ are 4×4 real matrices:

$$(\mathbf{Q})_{IK}=E_{1IK1},\quad (\mathbf{R})_{IK}=E_{1IK2},\quad (\mathbf{T})_{IK}=E_{2IK2}. \tag{17}$$

The eigenvectors $\mathbf{b}_j$ can be obtained from

$$\mathbf{b}_j=(\mathbf{R}^{\mathrm{T}}+p_j\mathbf{T})\mathbf{a}_j=-\frac{1}{p_j}(\mathbf{Q}+p_j\mathbf{R})\mathbf{a}_j. \tag{18}$$

Introduce a new matrix:

$$\mathbf{L}=\mathrm{i}\mathbf{A}\mathbf{B}^{-1}, \tag{19}$$

then the bi-material matrix $\mathbf{H}$ can be expressed as

$$\mathbf{H}=\mathbf{L}_1+\overline{\mathbf{L}}_2, \tag{20}$$

here $\mathbf{H}$ is also 4×4 complex matrix,

$$\mathbf{H}=[\mathbf{H}_1,\mathbf{H}_2,\mathbf{H}_3,\mathbf{H}_4]^{\mathrm{T}}. \tag{21}$$

2.2. Green's function for a single dislocation at the interface of two bonded piezoelectric materials

A framework solution for a single dislocation at the interface of anisotropic bimaterials has been carried out by Suo (1990). This solution method can be extended to the similar problem for piezoelectric bimaterials. Assuming the dislocation is in material 2, the lower material, the solution can be written as

$$\mathbf{f}(z)=\begin{cases}\mathbf{f}^1(z), & z\in 1,\\ \mathbf{f}^2(z)+\mathbf{f}_0(z), & z\in 2,\end{cases} \tag{22}$$

where the superscript refer to the materials, and $\mathbf{f}_0(z)$ is the dislocation solution for an infinite homogeneous medium given by

$$\mathbf{f}_0(z)=\mathbf{B}^{-1}(\mathbf{L}+\overline{\mathbf{L}})^{-1}\mathbf{b}\ln z, \tag{23}$$

in which $\mathbf{b}$ is the burgers vector of the dislocation defined as the jump across the interface,

$$\mathbf{b}=\mathbf{U}_1(x,0)-\mathbf{U}_2(x,0). \tag{24}$$

By considering stress and displacement continuity across the interface, Eq. (22) can be solved as

$$\begin{cases}\mathbf{f}^1(z)=\mathbf{B}_1^{-1}\mathbf{H}^{-1}(\overline{\mathbf{L}}_2+\mathbf{L}_2)\mathbf{B}_2\mathbf{f}_0(z) & z\in\text{material 1},\\ \mathbf{f}^2(z)=\mathbf{B}_2^{-1}\overline{\mathbf{H}}^{-1}(\overline{\mathbf{L}}_2-\mathbf{L}_1)\overline{\mathbf{B}}_2\bar{\mathbf{f}}_0(z) & z\in\text{material 2}.\end{cases} \tag{25}$$

When the dislocation locates at the interface (illustrated in Fig. 3), Eq. (25) is simplified to

$$\mathbf{B}_1\mathbf{f}_1(z)=\overline{\mathbf{B}}_2\bar{\mathbf{f}}_2(z)=\frac{1}{2\pi}\mathbf{H}^{-1}\mathbf{b}\ln z. \tag{26}$$

Therefore the SED is obtained from (11),

$$\Pi_{2i}=2\,\mathrm{Re}\left[\sum_{j=1}^{4}B_{ij}f_j'(z_j)\right]. \tag{27}$$

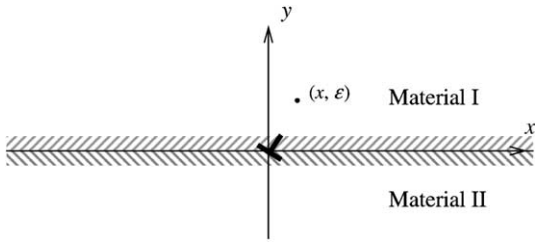

Fig. 3. A single dislocation at the metal/piezoelectric interface.

By substituting $z_j = x + p_j y$ into Eq. (27), we have

$$\Pi_{2i}(x,y) = \mathrm{Re}\left[\sum_{j=1}^{4} \frac{1}{\pi} H_{ij}^{-1} b_j \frac{1}{x + p_j y}\right], \tag{28}$$

where the traction along the interface is obtained from (28) by Suo (1990),

$$\Pi_{2i}(x,0) = \frac{1}{2\pi}\left(\frac{\mathbf{H}^{-1}}{x + 0\mathrm{i}} + \frac{\overline{\mathbf{H}}^{-1}}{x - 0\mathrm{i}}\right)\mathbf{b}, \tag{29}$$

in which $x + 0\mathrm{i}$ means a point approaching the x-axis from the upper half-plane while $x - 0\mathrm{i}$ is for the point from the lower half-plane. However when the solution (29) is employed as a Green function solution to investigate corresponding crack problem with the aid of distributed dislocation method, the integrals of the stress field of a single dislocation cannot be simply determined from Eq. (29), as stated by Suo (1990). To calculate the traction on the interface, the following limit is introduced (Qu and Li, 1991):

$$\lim_{y \to \pm 0}\left\{\frac{1}{x + p_j y}\right\} = \frac{1}{x} \mp \mathrm{i}\pi\delta(x), \quad \mathrm{Im}\{p_j\} > 0, \tag{30}$$

in which the delta function takes the form

$$\int_{-\infty}^{+\infty} \delta(x)\,\mathrm{d}x = 1, \tag{31}$$

$$\delta(x) = \begin{cases} 0, & |x| > 0, \\ \infty, & x = 0. \end{cases} \tag{32}$$

Generally, $\mathbf{H}$ is not a real matrix and is expressed as

$$\mathbf{H}^{-1} = \mathbf{M} + \mathrm{i}\mathbf{N} \tag{33}$$

with $\mathbf{M}$ and $\mathbf{N}$ being both real matrices.

Using Eqs. (30)–(33), Eq. (29) can be expressed as

$$\Pi_{2i}(x,0) = \sum_{j=1}^{4}\left[\frac{1}{\pi} M_{ij} b_j \frac{1}{x} + N_{ij} b_j \delta(x)\right]. \tag{34}$$

The difference of Eqs. (29) and (34) is the expression of the stress field at the dislocation core, which must be evaluated when the solution is applied for formulating a crack. The stress field for piezoelectric materials we obtained here is well consistent with that for general isotropic material (cf. Appendix A). With the distributed dislocation technique, this solution for a single dislocation can be immediately used to investigate

interaction problems between dislocations and cracks, as well as to formulate various types of interfacial crack problems.

2.3. The open model for the Zener–Stroh crack

As shown in Fig. 2, for an interfacial Zener–Stroh crack, the boundary conditions is expressed as

$$\mathbf{\Pi}^1_{2K} = \mathbf{\Pi}^2_{2K} = 0, \quad -a < x < a, \tag{35}$$

$$\mathbf{\Pi}^1_{2K} = \mathbf{\Pi}^2_{2K}, \quad |x| > a, \tag{36}$$

$$\mathbf{U}^1_K = \mathbf{U}^2_K, \quad |x| > a. \tag{37}$$

With the above boundary conditions, the stress field due to a Zener–Stroh crack can be obtained by integrating Eq. (34) along the crack line,

$$\Pi_{2i}(x,0) = \int_{-a}^{+a} \sum_{j=1}^{4} \left[\frac{1}{\pi} M_{ij} D_j(\xi) \frac{1}{x-\xi} + N_{ij} D_j(\xi) \delta(x) \right] \mathrm{d}\xi, \quad -a < x < a, \tag{38}$$

where $\mathbf{D}$ is the dislocation density,

$$\mathbf{D}(\xi) = \frac{\mathrm{d}\mathbf{b}(\xi)}{\mathrm{d}\xi}. \tag{39}$$

Considering the characteristic of the delta function mentioned above, the equation is changed to

$$\Pi_{2k}(x,0) = \int_{-a}^{+a} \sum_{j=1}^{4} \frac{1}{\pi} M_{ij} D_j(\xi) \frac{1}{x-\xi} \, \mathrm{d}\xi + \sum_{j=1}^{4} N_{ij} D_j(x), \quad -a < x < a. \tag{40}$$

For the current study, we consider a purely displacement loaded Zener–Stroh crack. The net total dislocations inside the crack are not equal to zero but

$$\int_{-a}^{+a} \mathbf{D}(\xi) \, \mathrm{d}\xi = \mathbf{b}^{\mathrm{T}}. \tag{41}$$

Combining Eqs. (40) and (41), the problem can be solved numerically with the numerical method given in Section 3.

2.4. Contact zone model for the Zener–Stroh crack

In this section, the physical problem considered is the same as the one in Fig. 2. But for the current formulation, in order to cease the oscillation phenomenon for the stress and displacement solution near the crack tip, a contact zone behind the right crack tip is introduced based on Comninou (1977). The length of the contact zone is $a - b$ as shown in Fig. 4. This means inside the contact zone, the upper and lower crack faces touch each other. As a result, the boundary conditions are changed to:

$$\mathbf{\Pi}^1_{22} = \mathbf{\Pi}^2_{22} = 0, \quad -a < x < b, \tag{42}$$

$$\mathbf{\Pi}^1_{2K} = \mathbf{\Pi}^2_{2K} = 0, \quad -a < x < a, \;\; K = 1,3,4, \tag{43}$$

$$\mathbf{\Pi}^1_{2K} = \mathbf{\Pi}^2_{2K}, \quad |x| > a, \tag{44}$$

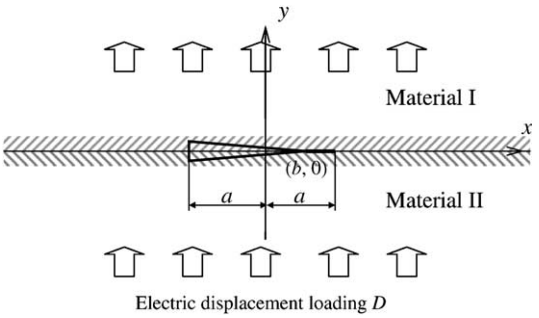

Fig. 4. The contact zone model for the current interfacial Zener–Stroh crack.

$$\mathbf{U}_K^1 = \mathbf{U}_K^2, \quad |x| > a. \tag{45}$$

Taking consideration of Eq. (42), the normal stress field of the Zener–Stroh crack along the interface outside the contact zone, i.e., $-a < x < b$, is expressed as

$$\begin{aligned} \Pi_{22}(x,0) = &\int_{-a}^{+b} \left[\frac{1}{\pi} M_{22} D_2(\xi) \frac{1}{x-\xi} + N_{22} D_2(\xi)\delta(x)\right] \mathrm{d}\xi \\ &+ \int_{-a}^{+a} \sum_{j=1,2,3} \left[\frac{1}{\pi} M_{2j} D_j(\xi) \frac{1}{x-\xi} + N_{2j} D_j(\xi)\delta(x)\right] \mathrm{d}\xi, \quad -a < x < b. \end{aligned} \tag{46}$$

When $-a < x < a$, Eq. (43) for the shear stress becomes

$$\begin{aligned} \Pi_{2i}(x,0) = &\int_{-a}^{+b} \left[\frac{1}{\pi} M_{i2} D_2(\xi) \frac{1}{x-\xi} + N_{i2} D_2(\xi)\delta(x)\right] \mathrm{d}\xi \\ &+ \int_{-a}^{+a} \sum_{j=1,2,3} \left[\frac{1}{\pi} M_{ij} D_j(\xi) \frac{1}{x-\xi} + N_{ij} D_j(\xi)\delta(x)\right] \mathrm{d}\xi, \quad -a < x < a, \ \text{for } i = 1,3,4. \end{aligned} \tag{47}$$

By integrating the second parts in the square brackets of the above two equations, and considering the characteristic of delta function, we obtain

$$\begin{aligned} \Pi_{22}(x,0) = &\int_{-a}^{+b} \frac{1}{\pi} M_{22} D_2(\xi) \frac{1}{x-\xi} \,\mathrm{d}\xi + \Lambda(\cdot) N_{22} D_2(x) + \int_{-a}^{+a} \frac{1}{\pi} \sum_{j=1,3,4} M_{2j} D_j(\xi) \frac{1}{x-\xi} \,\mathrm{d}\xi \\ &+ \sum_{j=1,3,4} N_{2j} D_2(x), \quad -a < x < b, \end{aligned} \tag{48}$$

$$\begin{aligned} \Pi_{2i}(x,0) = &\int_{-a}^{+b} \frac{1}{\pi} M_{i2} D_2(\xi) \frac{1}{x-\xi} \,\mathrm{d}\xi + \Lambda(\cdot) N_{i2} D_2(x) + \int_{-a}^{+a} \frac{1}{\pi} \sum_{j=1,3,4} M_{ij} D_j(\xi) \frac{1}{x-\xi} \,\mathrm{d}\xi \\ &+ \sum_{j=1,3,4} N_{ij} D_2(x), \quad -a < x < a, \ \text{for } i = 1,3,4, \end{aligned} \tag{49}$$

where $\Lambda(\cdot)$ is the Heaviside step function to ensure that D_2 is included only in the shear equation for $-a < x < b$,

$$\Lambda(\cdot) = \Lambda(x+a) - \Lambda(x-b). \tag{50}$$

Similar to the open model in Section 2.3, the net dislocations are not equal to zero, but

$$\int_{-a}^{+b} D_2(\xi)\,\mathrm{d}\xi = b_2^{\mathrm{T}}, \tag{51}$$

$$\int_{-a}^{+a} D_j(\xi)\,\mathrm{d}\xi = b_j^{\mathrm{T}}, \quad j = 1,3,4. \tag{52}$$

2.5. Nature of singularities at the crack tips

As mentioned above, one of the Zener–Stroh crack tips where dislocations enter the crack is called blunt tip, and the other one is called the sharp tip. The crack tip singularities of a Zener–Stroh crack are different for fully open crack tip model and contact zone model. The singularities of the crack tip are related to the behavior of the dislocation density **D** which can be expressed as

$$\mathbf{D}(x) = \frac{\mathrm{d}}{\mathrm{d}x}[\mathbf{U}^{+}(x) - \mathbf{U}^{-}(x)]. \tag{53}$$

Comninou (1977) gave an analysis for an interfacial Griffith crack in isotropic bimaterials with contact zone model. Following her analysis, Fan et al. (1998) presented that only the components of dislocation density in x-direction is bounded at $(b,0)$ while others are all singular at the crack tips for a Zener–Stroh crack with the contact zone model. This analysis can also be applied to piezoelectric anisotropic bimaterials. For the open crack tip model, all dislocation density **D**'s will be singular at both crack tips. While for the contact zone model, $\mathbf{D}_2$ is bounded at $(b,0)$ and the other **D**'s are all singular at both crack tips. For each case, the dislocation density may be written as

$$\mathbf{D}(s) = \omega(s)\boldsymbol{\Psi}(s), \tag{54}$$

where $\boldsymbol{\Psi}(s)$ is a bounded function and $\omega(s)$ is the corresponding fundamental function for Cauchy kernels. According to the above singularity analysis, $\omega(s)$ can be chosen from Hills et al.'s (1996) book according to different singularities.

For open crack tip model:

$$\mathbf{D}(s) = \frac{\boldsymbol{\Xi}(s)}{(1-s^2)^{1/2}}; \tag{55}$$

For contact zone model:

$$D_2(s) = \frac{(1-s)^{1/2}}{(1+s)^{1/2}}\Xi_2(s), \tag{56}$$

$$D_j(s) = \frac{\Xi_j(s)}{(1-s^2)^{1/2}}, \quad j = 1,3,4, \tag{57}$$

where $\boldsymbol{\Xi}(s)$ $(= [\Xi_1(s), \Xi_2(s), \Xi_3(s), \Xi_4(s)])$ are unknown functions which are bounded and continuous in the interval $(-a,a)$.

As a Zener–Stroh crack always propagates from its sharp crack tip (right crack tip in the current problem), only the SEDIFs of the right crack tip should be evaluated, which takes the form as

$$\mathbf{K} = [K_{\mathrm{II}}, K_{\mathrm{I}}, K_{\mathrm{III}}, K_{\mathrm{D}}]^{\mathrm{T}} = \lim_{x\to a}\sqrt{2\pi(x-a)}\boldsymbol{\Pi}_2(x,0). \tag{58}$$

3. Numerical procedure

The singular integral equations we have set up for the physical problem can be solved numerically by using Erdogan and Gupta's method (Erdogan and Gupta, 1972) and Krenk's interpolation formulae (Krenk, 1975). The crack length is normalised to a unit without influencing the analytical results, i.e.,

$$a = 1, \quad b \leqslant 1. \tag{59}$$

Because the singularities for the open model and the contact model are substantially different, their numerical procedures are given respectively.

3.1. The open model

For the open model, Eqs. (40) and (41) are changed to

$$\Pi_{2i}(x,0) = \int_{-1}^{+1} \sum_{j=1}^{4} \frac{1}{\pi} M_{ij} D_j(\xi) \frac{1}{x-\xi} \,\mathrm{d}\xi + \sum_{j=1}^{4} N_{ij} D_j(x), \quad -1 < x < 1, \tag{60}$$

$$\int_{-1}^{+1} \mathbf{D}(\xi)\mathrm{d}\xi = \mathbf{b}^{\mathrm{T}}. \tag{61}$$

The discretized forms of singular equations (60) and (61) are

$$\Pi_{2i}(x_m,0) = \sum_{k=1}^{N} \left\{ \frac{1}{N} \sum_{j=1}^{4} M_{ij} \frac{\Xi(\xi_k)}{x_m - \xi_k} + \sum_{j=1}^{4} \frac{2}{N} N_{ij} \frac{1}{(1-\xi_k^2)^{1/2}} \Theta(x_m)\Xi(\xi_k) \right\}, \quad m = 1, \ldots, N-1, \tag{62}$$

$$\frac{\pi}{N} \sum_{k=1}^{N} \Xi(\xi_k) = \mathbf{b}^{\mathrm{T}}, \tag{63}$$

where

$$\Theta(x_m) = \frac{1}{2} + \sum_{l=1}^{N-1} \cos\left(\frac{2k-1}{2N} l\pi\right) \cos(l\gamma), \quad \gamma = \arccos(x_m), \tag{64}$$

$$\xi_k = \cos\left(\pi \frac{2k-1}{2N}\right), \quad x_m = \cos\left(\pi \frac{m}{N}\right), \tag{65}$$

There are totally $4N$ unknowns in the linear equation systems (62) and (63) which have $4N$ linear equations, so the equation system can be solved uniquely. After we obtain the solutions of the unknowns, we can substitute them into the following equations to obtain the SED field along the interface:

$$\Pi_{2i}(x,0) = \sum_{k=1}^{N} \left\{ \frac{1}{N} \sum_{j=1}^{4} M_{ij} \frac{\Xi(\xi_k)}{x-\xi_k} + \sum_{j=1}^{4} \frac{2}{N} \frac{1}{1-\xi_k^2} N_{ij} \Theta(x)\Xi(\xi_k) \right\}. \tag{66}$$

The SEDIFs can be obtained through the limit calculation and numerical treatment. This procedure can be found in Hills et al.'s (1996) book. The stress intensity factors (SIFs) for general anisotropic bimaterials were discussed by Huang and Kardomateas (2001) in a similar way. Based on this procedure, the current results for the SEDIFs are given by

$$K_i = \sum_{j=1}^{4} \left\{ [M_{ij} + N_{ij}]\sqrt{\pi}\frac{1}{N}\sum_{i=1}^{N} \frac{\sin\left[\frac{2i-1}{4N}\pi(2N-1)\right]}{\sin\left[\frac{2i-1}{4N}\pi\right]} \Xi(\xi_i) \right\}. \tag{67}$$

3.2. The contact zone model

As we mentioned earlier, for this model, there is a contact zone behind the sharp crack tip. To normalize all the integral ranges to $(-1, 1)$, we introduce the following transformation:

$$t = \frac{2x}{b+1} - \frac{b-1}{b+1}, \quad \text{when } -1 < x < b, \tag{68}$$

$$s = \frac{2\xi}{b+1} - \frac{b-1}{b+1}, \quad \text{when } -1 < \xi < b, \tag{69}$$

$$\xi = \frac{b-1}{2} + \frac{b+1}{2}s, \quad -1 < s < 1, \tag{70}$$

$$x = \frac{b-1}{2} + \frac{b+1}{2}t, \quad -1 < t < 1, \tag{71}$$

and Eqs. (48), (49), (51) and (52) are changed to

$$\begin{aligned} \Pi_{22}(x,0) = {} & \int_{-1}^{+1} \frac{1}{\pi} M_{22} D_2(s) \frac{1}{t-s}\,\mathrm{d}s + \Lambda(\cdot) N_{22} D_2(t) + \int_{-1}^{+1} \frac{1}{\pi} \sum_{j=1,3,4} M_{2j} D_j(\xi) \frac{1}{x-\xi}\,\mathrm{d}\xi \\ & + \sum_{j=1,3,4} N_{2j} D_j(x), \quad -1 < t < 1, \end{aligned} \tag{72}$$

$$\begin{aligned} \Pi_{2i}(x,0) = {} & \int_{-1}^{+1} \frac{1}{\pi} M_{i2} D_2(s) \frac{1}{t-s}\,\mathrm{d}s + \Lambda(\cdot) N_{i2} D_2(t) + \int_{-1}^{+1} \frac{1}{\pi} \sum_{j=1,3,4} M_{ij} D_j(\xi) \frac{1}{x-\xi}\,\mathrm{d}\xi \\ & + \sum_{j=1,3,4} N_{ij} D_j(x), \quad -1 < x < 1, \ \text{for } i = 1,3,4, \end{aligned} \tag{73}$$

$$\frac{b+1}{2} \int_{-1}^{+1} D_2(s)\,\mathrm{d}s = b_2^{\mathrm{T}}, \tag{74}$$

$$\int_{-1}^{+1} D_i(\xi)\mathrm{d}\xi = b_i^{\mathrm{T}}, \ i = 1,3,4. \tag{75}$$

The discretized form of Eqs. (72)–(75) are:

$$\Pi_{22}(x_m,0) = \sum_{k=1}^{N} \left\{ \begin{array}{l} M_{22} \frac{2(1-s_k)}{2N+1} \frac{\Xi_2(s_k)}{t_m - s_k} \\ \quad + \Lambda(\cdot) \frac{4}{2N+1} N_{22} \Omega\left(\frac{2x_m}{1+b} - \frac{b-1}{b+1}\right) \Xi_2(s_k) \frac{\left[1-\left(\frac{2x_m}{1+b} - \frac{b-1}{b+1}\right)\right]^{1/2}}{\left[1+\left(\frac{2x_m}{1+b} - \frac{b-1}{b+1}\right)\right]^{1/2}} \\ \quad + \sum_{j=1,3,4} \left[\frac{1}{N} M_{2j} \frac{\Xi_j(\xi_k)}{x_m - \xi_k}\right] \\ \quad + \sum_{j=1,3,4} \frac{2}{N} N_{2j} \Theta\left(\frac{1+b}{2} t_m - \frac{1-b}{2}\right) \Xi_j(\xi_k) \left[1 - \left(\frac{1+b}{2} t_m - \frac{1-b}{2}\right)^2\right]^{1/2} \end{array} \right\}, \\ m = 1, \ldots, N, \end{aligned} \tag{76}$$

$$\Pi_{2i}(x_m,0)=\sum_{k=1}^{N}\left\{\begin{array}{l} M_{i2}\frac{2(1-s_k)}{2N+1}\frac{\Xi_2(s_k)}{t_m-s_k} \\ \quad +\Lambda(\cdot)\frac{4}{2N+1}N_{i2}\Omega\left(\frac{2x_m}{1+b}-\frac{b-1}{b+1}\right)\Xi_2(s_k)\frac{\left[1-\left(\frac{2x_m}{1+b}-\frac{b-1}{b+1}\right)\right]^{1/2}}{\left[1+\left(\frac{2x_m}{1+b}-\frac{b-1}{b+1}\right)\right]^{1/2}} \\ \quad +\sum_{j=1,3,4}\left[\frac{1}{N}M_{ij}\frac{\Xi_j(\xi_k)}{x_m-\xi_k}\right] \\ \quad +\sum_{j=1,3,4}\frac{2}{N}N_{ij}\Theta\left(\frac{1+b}{2}t_m-\frac{1-b}{2}\right)\Xi_j(\xi_k)\left[1-\left(\frac{1+b}{2}t_m-\frac{1-b}{2}\right)^2\right]^{1/2} \end{array}\right\},$$

$$m=1,\ldots,N-1,\quad \text{for } i=1,3,4, \tag{77}$$

$$\frac{2\pi}{2N+1}\frac{b+1}{2}\sum_{k=1}^{N}\Xi_2(s_k)=b_2^{\mathrm{T}}, \tag{78}$$

$$\frac{\pi}{N}\sum_{k=1}^{N}\Xi_i(\xi_k)=b_i^{\mathrm{T}}\quad \text{for } i=1,3,4, \tag{79}$$

where

$$\Omega(s)=\sum_{l=0}^{N-1}\sin\left[\frac{k\pi}{2N+1}\right]\sin\left[\frac{k\pi}{2N+1}(2l+1)\right]\frac{\sin[2(l+1)\gamma]}{\sin\gamma}\quad \text{with } \gamma=\arccos\left(\sqrt{\frac{1+s}{2}}\right), \tag{80}$$

$$\Theta(s)=\frac{1}{2}+\sum_{l=1}^{N-1}\cos\left(\frac{2k-1}{2N}l\pi\right)\cos(l\gamma)\quad \text{with } \gamma=\arccos(s), \tag{81}$$

$$s_k=\cos\left(\pi\frac{2k}{2N+1}\right),\quad t_m=\cos\left(\pi\frac{2m-1}{2N+1}\right), \tag{82}$$

$$\xi_k=\cos\left(\pi\frac{2k-1}{2N}\right),\quad x_m=\cos\left(\pi\frac{m}{N}\right), \tag{83}$$

Equation systems (76)–(79) contain $4N+1$ equations with $4N+1$ unknowns, and can be solved uniquely. Different to equation systems (62) and (63), however, these equations are nonlinear with the parameter b. Iteration calculating procedure should be taken. We first specify an estimated value of b and the $4N$ equations become linear and the $4N$ unknowns can be obtained. Then the obtained $4N$ unknowns are substituted into the objective equation to test if it is satisfied. New values of b are chosen using secant method and the process is repeated until the precision of the objective equation reaches a certain degree.

After the equation systems are solved, the SEDIFs can be calculated with the following equations:

$$K_i=\sum_{j=1,3,4}\left\{[M_{ij}+N_{ij}]\sqrt{\pi}\frac{1}{N}\sum_{i=1}^{N}\frac{\sin\left[\frac{2i-1}{4N}\pi(2N-1)\right]}{\sin\left[\frac{2i-1}{4N}\pi\right]}\Xi_j(\xi_i)\right\}. \tag{84}$$

4. Numerical examples and related results

The two materials selected for calculation are lead zirconate titanate (PZT-5H) and platinum (Pt), whose material properties are listed in Tables 1 and 2, respectively. For plane strain problem, we set $b_3^{\mathrm{T}}=0$ and $b_4^{\mathrm{T}}=0$ and only b_x^{T} and b_y^{T} are considered. To emphasize the Zener–Stroh crack mechanism, we assume

Table 1
Material properties of PZT-5H ceramics (Pak, 1992)

c_{11}	c_{12}	c_{13}	c_{22}	c_{44}	e_{16}	e_{21}	e_{34}	κ_{11}	κ_{22}
126 GPa	53 GPa	55 GPa	117 GPa	35.3 GPa	17 C/m^2	−6.5 C/m^2	23.3 C/m^2	151×10^{-10} C/Vm	130×10^{-10} C/Vm

The polarized direction is along the y-axis.

Table 2
Material properties of platinum (Pt)

Young's modulus (GPa)	Poisson's ratio
145	0.38

there is no far field stress loading, while the far field electric load is considered. Results obtained are compared with those without electric field in order to reveal the electro-elastics characteristics of Zener–Stroh crack in piezoelectric materials. It is worth to mention that if there are far field mechanical loads applied, the stress fields due to these loads can be superposed directly to the current solution.

4.1. Contact zone length

For the contact zone model in absent of electric field, the variation of the contact zone length $(1-b)$ with the total burgers vectors is illustrated in Fig. 5. It is found that when the displacement loading ratio $b_y^{\mathrm{T}}/b_x^{\mathrm{T}}$ increases, the contact zone length $1-b$ decreases. This means that if b_x^{T} is very small, the contact zone can be ignored. While when b_x^{T} increases, the contact zone length also increases. This result indicates that the contact zone length is shear-loading dominated. Therefore the crack must be reformulated into the open crack tip model when the shear displacement loading b_x^{T} is relatively small. The result is consistent to that for Zener–Stroh crack and Griffth crack at the interface of dissimilar isotropic bimaterials (Fan et al., 1998; Comninou and Schmueser, 1979). The variation of electric displacement **D** with the displacement load $b_y^{\mathrm{T}}/b_x^{\mathrm{T}}$ is plotted in Fig. 6. It is seen that the electric displacement has a linear relation with the displacement

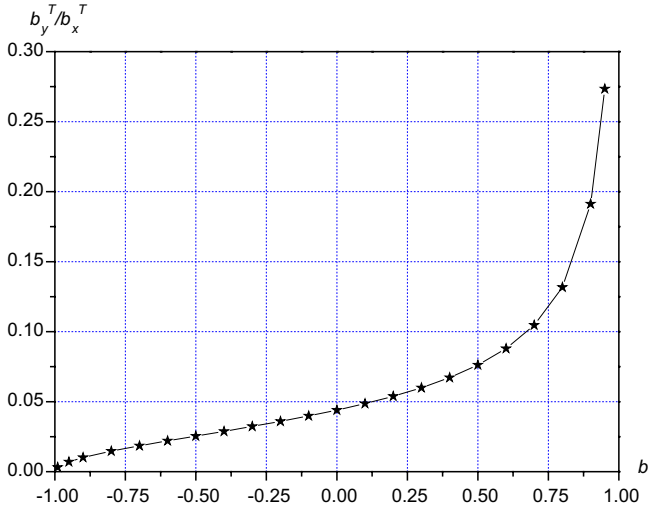

Fig. 5. Contact zone length versus total Burgers vectors without electric field applied.

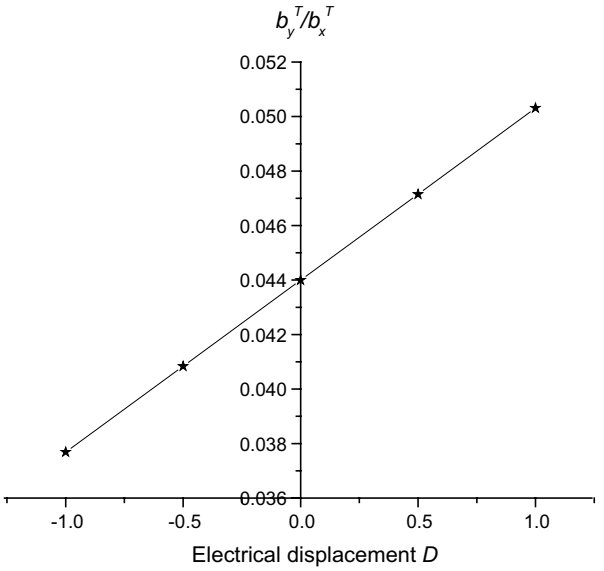

Fig. 6. The relation between the electric displacement and $b_y^{\mathrm{T}}/b_x^{\mathrm{T}}$ for a given contact zone length $1-b=1$.

loading when the contact zone length is specified, which indicates that these two types of loads work together to determine the contact zone length.

4.2. Stress and electric displacement intensity factors

For plane strain problem, $K_{\mathrm{III}}=0$, only the SIFs K_{I}, K_{II} and the EDIFs K_{D} are considered. Figs. 7–9 show the SEDIFs obtained from both contact zone model and open crack tip model in the condition of no

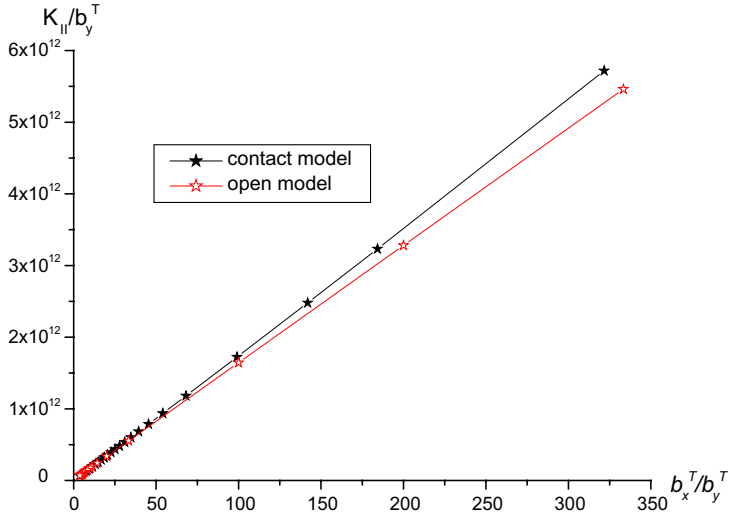

Fig. 7. Stress intensity factors K_{II} versus total Burgers vectors when no electric field is applied.

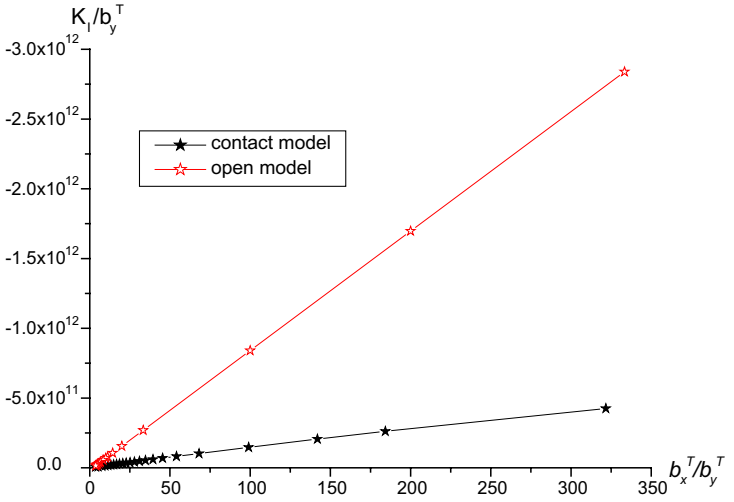

Fig. 8. Stress intensity factors K_I versus total Burgers vectors when no electric field is applied.

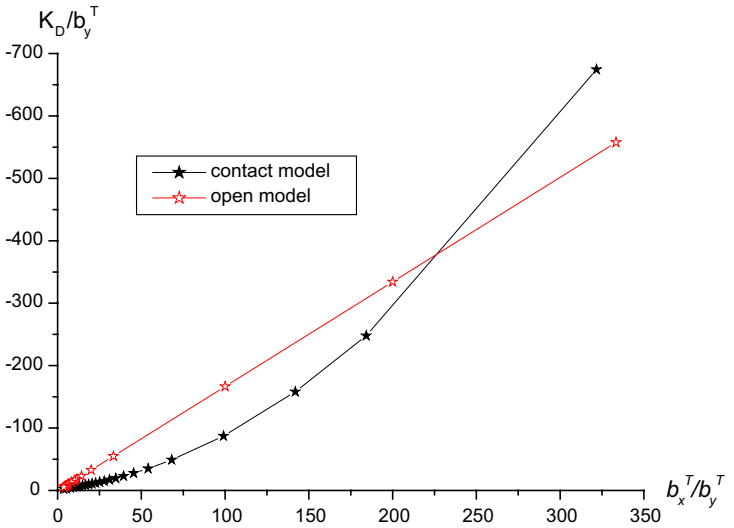

Fig. 9. Electric displacement intensity factors K_D versus total Burgers vectors when no electric field is applied.

electric field applied. From Fig. 7, it is found that the values due to both contact model and open crack tip model have only a small difference for K_{II} While in Fig. 8, the difference of K_I between these two models becomes much larger when the shearing displacement loading (b_x^T) increases. As mentioned above, larger shear loading will bring larger contact zone length. This means contact zone length has large influence on K_I but not on K_{II}. The current results for both K_I and K_{II} are consistent with those for Griffith crack case. The electric displacement intensity factors calculated from the two models is plotted in Fig. 9 where no electric field is applied. It is observed that for the open crack tip model, the value of K_D is proportional to the displacement loading; While for the contact zone model, K_D also increases with the displacement loading,

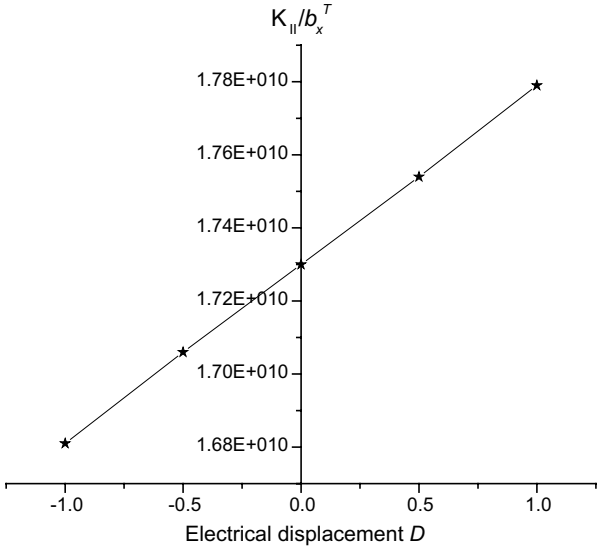

Fig. 10. K_{II} versus the electric displacement loading for a given contact zone length $1 - b = 1$.

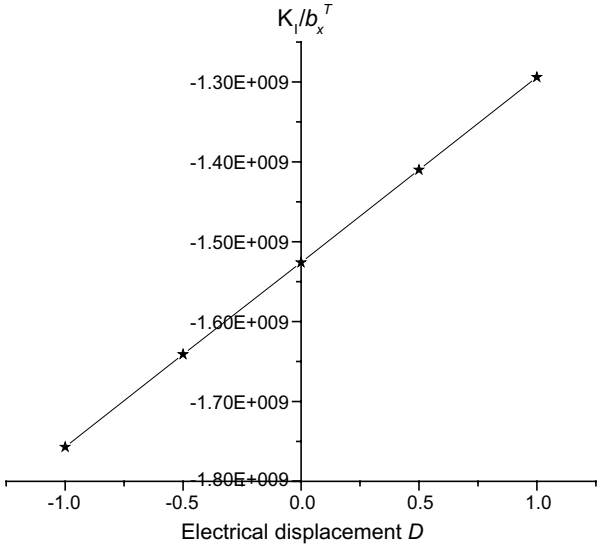

Fig. 11. K_I versus the electric displacement loading for a given contact zone length $1 - b = 1$.

but not linearly. This is due to the fact that with the introducing of the contact zone, the problem is no more linear.

The influences of the electric displacement loading on SEDIFs are shown in Figs. 10–12. It is seen that the SIFs and EDIFs are all linearly proportional to the electric displacement loading. It is noted that the electric displacement loading can weaken or strengthen the SIFs and EDIFs, depending on the electric field direction. Particularly the influence of the applied electric field on EDIFs is critical. In Fig. 12, it is observed that the EDIFs can be reduced greatly (even to negative) by the electric loading.

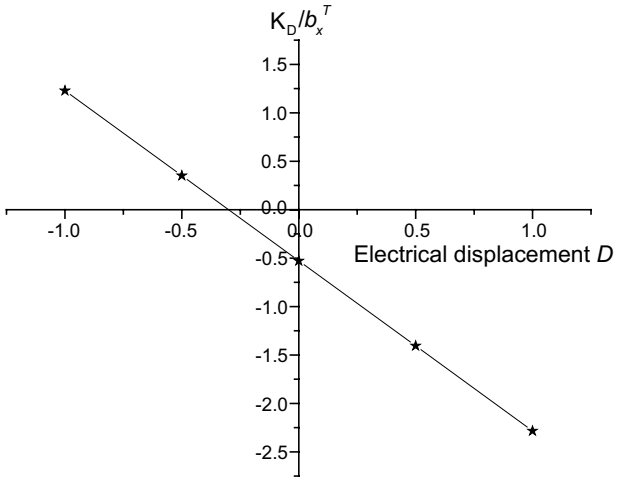

Fig. 12. K_D versus the electric displacement loading for a given contact zone length $1 - b = 1$.

5. Conclusions

The physical problem of a Zener–Stroh crack at the interface of metal/piezoelectric bimaterial has been investigated with both open crack tip model and contact zone model. Some concluding remarks can be drawn:

(1) The SEDIFs based on the open crack tip model and contact zone model have fairly large differences, when the shear displacement loading is dominant. This result indicates that the contact zone model should be used if the shear loading applied is large.
(2) A pure displacement loading (the total burgers vectors inside a Zener-Stroch crack for the current case) can also bring electric displacement intensity factors, since one of the materials is piezoelectric.
(3) The electric field applied can prevent or enhance the propagation and nucleation of a Zener–Stroh crack by adjusting the applied direction. Particularly the influence of the electric loading on the electric displacement intensity factors is much larger that that on the stress intensity factors.

Appendix A. The stress field due to an interfacial dislocation

Eq. (34) could be degenerated to the stress field for dissimilar isotropic bimaterials if we substitute the bimaterial matrix **H** for isotropic material into it. **H** is in forms of (Suo et al., 1992)

$$\mathbf{H} = \begin{bmatrix} \frac{1-v}{\mu} & \mathrm{i}\left(\frac{1-2v}{2\mu}\right) & 0 & 0 \\ -\mathrm{i}\left(\frac{1-2v}{2\mu}\right) & \frac{1-v}{\mu} & 0 & 0 \\ 0 & 0 & \frac{1}{\mu} & 0 \\ 0 & 0 & 0 & -\frac{1}{\kappa} \end{bmatrix}, \tag{A.1}$$

where $\kappa = \infty$ for conductors, and therefore Eq. (34) is changed to

$$\sigma_{yy}(x,0) = -\beta C b_x \delta(x) + C b_y \frac{1}{x}, \tag{A.2}$$

$$\sigma_{xy}(x,0) = Cb_x \frac{1}{x} + \beta Cb_y \delta(x), \tag{A.3}$$

in which C is the bi-material constant, for plane strain its value is

$$C = \frac{4\mu_1\mu_2(\mu_1+\mu_2-\mu_1\nu_2-\mu_2\nu_1)}{(\mu_1+3\mu_2-4\mu_2\nu_1)(\mu_2+3\mu_1-4\mu_1\nu_2)}. \tag{A.4}$$

Eqs. (A.2) and (A.3) has been employed to investigate interfacial Zener–Stroh crack in general isotropic bimaterials (Fan et al., 1998), and the formulation can be obtained from the degeneration of Eqs. (48)–(52).

References

Cherepanov, G.P., 1994. Interface microcrack nucleation. Journal of the Mechanics and Physics of Solids 42, 665–680.

Comninou, M., 1977. The interface cracks. ASME Journal of Applied Mechanics 44, 631–636.

Comninou, M., Schmueser, D., 1979. The interface crack in a combined tension–compression and shear field. ASEM Journal of Applied Mechanics 46, 345–348.

Cottrell, A.H., 1958. Theory of brittle fracture in steel and similar metals. Transaction of the Metallurgical Society of the AIME 212, 192–203.

Erdogan, F., Gupta, G.D., 1972. On the numerical solution of singular integral equations. Quarterly of Applied Mathematics 30, 525–534.

Fan, H., 1994. Interfacial Zener–Stroh crack. Journal of Applied Mechanics 61, 829–834.

Fan, H., Sun, Y.M., Xiao, Z.M., 1998. Contact zone in an interfacial Zener–Stroh crack. Mechanics of Materials 30, 151–159.

Gao, C.F., Yu, J.H., 1998. Two-dimensional analysis of a semi-infinite crack in piezoelectric media. Mechanics Research Communications 25, 695–700.

Hills, D.A., Kelly, P.A., Dai, D.N., Korsunsky, A.M., 1996. Solution of Crack Problems, The Distributed Dislocation Technique. Kluwer Academic Publishers.

Huang, H., Kardomateas, G.A., 2001. Mixed-mode stress intensity factors for cracks located at or parallel to the interface in bimaterial half planes. International Journal of Solids and Structures 38, 3719–3734.

Huang, Z., Kuang, Z.-B., 2001. Dislocation inside a piezoelectric media with an elliptic inhomogeneity. International Journal of Solids and Structures 38, 8459–8479.

Kikuchi, M., Shiozawa, K., Weertman, J.R., 1981. Void nucleation in astrology. Acta Metallurgica 29, 1747–1758.

Krenk, S., 1975. On the use of the interpolation polynomial for solutions of singular integral equations. Quarterly of Applied Mathematics 32, 479–484.

Lawson, L., Chen, E.Y., Meshii, M., 1997. Microstructural fracture in metal fatigue. International Journal of Fatigue 19, S61–S67.

Lekhnitskii, S.G., 1963. Theory of Elasticity of an Anisotropic Elastic Body. Holden-Day, San Francisco.

Pak, Y.E., 1992. Linear electro-elastic fracture mechanics of piezoelectric materials. International Journal of Fracture 54, 79–100.

Park, S.B., Sun, C.T., 1995. Effect of electric field on fracture of piezoelectric ceramics. International Journal of Fracture 70, 203–216.

Qin, Q.H., Mai, Y.W., 1998. Thermoelectroelastic Green's function and its application for bimaterial of piezoelectric materials. Archive of Applied Mechanics 68, 433–444.

Qin, Q.H., Yu, S.W., 1997. An arbitrarily-oriented plane crack terminating at the interface between dissimilar piezoelectric materials. International Journal of Solids and Structures 34, 581–590.

Qu, J., Li, Q., 1991. Interfacial dislocation and its applications to interface cracks in anisotropic bimaterials. Journal of Elasticity 26, 169–195.

Shen, S., Nishioka, T., Hu, S.L., 2000. Crack propagation along the interface of piezoelectric bimaterial. Theoretical and Applied Fracture Mechanics 34, 185–203.

Shih, C.J., Meyers, M.A., Nesterenko, V.F., Chen, S.J., 2000. Damage evolution in dynamic deformation of silicon carbide. Acta Materialia 48, 2399–2420.

Sosa, H., 1992. On the fracture mechanics of piezoelectric solids. International Journal of Solids and Structures 29, 2613–2622.

Stroh, A.N., 1954. The formation of cracks as a result of plastic flow, I. Proceedings of the Royal Society of London Series A 223, 404–414.

Stroh, A.N., 1955. The formation of cracks as a result of plastic flow, II. Proceedings of the Royal Society of London Series A 232, 548–560.

Stroh, A.N., 1958. Dislocations and cracks in anisotropic elasticity. Philosophical Magazine 7, 625–646.

Suo, Z., 1990. Singularities, interfaces and cracks in dissimilar anisotropic media. Proceedings of the Royal Society of London Series A—Mathematical and Physical Sciences 427, 331–358.

Suo, Z., Kuo, C.M., Barnett, D.M., Willis, J.R., 1992. Fracture mechanics for piezoelectric ceramics. Journal of Mechanics: Physics and Solids 40, 739–765.

Weertman, J.R., 1986. Zener–Stroh crack, Zener–Hollomon parameter, and other topics. Journal of Applied Physics 60, 1877–1887.

Xiao, Z.M., Chen, B.J., 2001. Stress analysis for a Zener–Stroh crack interacting with a coated inclusion. International Journal of Solids and Structures 38, 5007–5018.

Xiao, Z.M., Zhao, J.F., submitted for publication. A Zener–Stroh crack at the interface of a thin film bonded to a substrate.

Zener, C., 1948. The micro-mechanism of fracture. In: Fracturing of Metals. American Society of Metals, Cleveland. pp. 3–31.

Zhang, T.Y., Tong, P., 1996. Fracture mechanics for a mode III crack in a piezoelectric material. International Journal of Solids and Structures 33, 343–359.